THE JOURNAL OF PHYSICAL CHEMISTRY A
A JOURNAL OF THE AMERICAN CHEMICAL SOCIETY

pubs.acs.org/JPCA Article

Synthesis, Purification, and Rotational Spectroscopy of (Cyanomethylene)Cyclopropane—An Isomer of Pyridine

Brian J. Esselman, Samuel M. Kougias, Maria A. Zdanovskaia, R. Claude Woods,* and Robert J. McMahon*

Cite This: *J. Phys. Chem. A* 2021, 125, 5601−5614 Read Online

ACCESS | Metrics & More | Article Recommendations | Supporting Information

ABSTRACT: The gas-phase rotational spectrum of (cyanomethylene)cyclopropane, $(CH_2)_2C{=}CHCN$, generated by a Wittig reaction between the hemiketal of cyclopropanone and (cyanomethylene)triphenylphosphorane, is presented for the first time. This small, highly polar nitrile is a cyclopropyl-containing structural isomer of pyridine. The rotational spectra of the ground state and two vibrationally excited states were observed, analyzed, and least-squares fit from 130 to 360 GHz. Over 3900 R-, P-, and Q-branch, ground-state rotational transitions were fit to low-error, partial octic, A- and S-reduced Hamiltonians, providing precise determinations of the spectroscopic constants. The two lowest-energy vibrationally excited states, ν_{17} and ν_{27}, form a Coriolis-coupled dyad displaying small *a*- and *b*-type resonances. Transitions for these two states were measured and least-squares fit to a two-state, partial octic, A-reduced Hamiltonian in the I^r representation with nine Coriolis-coupling terms (G_a, G_a^J, G_a^K, G_a^{JJ}, F_{bc}, F_{bc}^J, F_{bc}^K, G_b, and G_b^J). The observation of many resonant transitions and nine nominal interstate transitions enabled a very accurate and precise energy difference between ν_{17} and ν_{27} to be determined: $\Delta E_{17,27}$ = 29.8975453 (33) cm^{-1}. The spectroscopic constants presented herein provide the foundation for future astronomical searches for (cyanomethylene)cyclopropane.

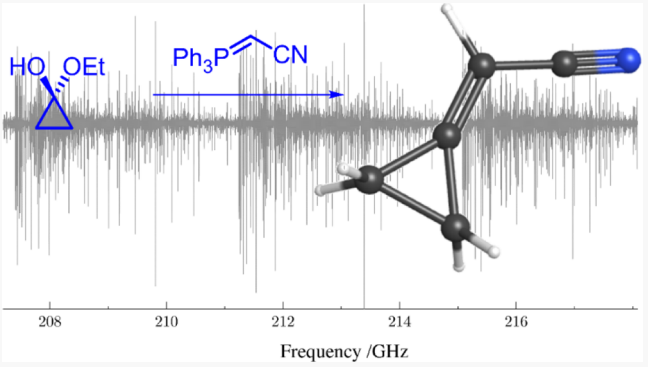

INTRODUCTION

Organic nitriles occupy a significant place in the field of astrochemistry and are well represented in the list of ∼220 species detected in space.[1,2] Their large molecular dipole moments, due to the cyano moiety, result in intense rotational transitions that facilitate identification of these species by radioastronomy. We have been keenly interested in measuring spectroscopic constants of organic nitriles in two groups: aryl nitriles/isonitriles[3−6] and nitrile-containing isomers of pyridine.[7−9] The former group was inspired by the potential of these aryl species to serve as tracers for their parent compounds (*e.g.*, benzene, pyridine, pyridazine, pyrimidine, and pyrazine). While pyridine, pyridazine, and pyrimidine possess a permanent dipole moment and have been sought in the interstellar medium unsuccessfully,[10] benzene and pyrazine do not and thus cannot be detected by radioastronomy. Recent detections of benzonitrile,[11] 1- and 2-cyanonaphthalene,[12] and 1-cyano-1,3-cyclopentadiene[13] represent a dramatic breakthrough in the field and have further inspired our spectroscopy of related compounds. The latter group of molecules that we have been studying are nitrile-containing structural isomers of pyridine (C_5H_5N) (Figure 1). Several of these species are likely to be involved in complex, astrochemically relevant processes[14,15] and have been detected in harsh reaction

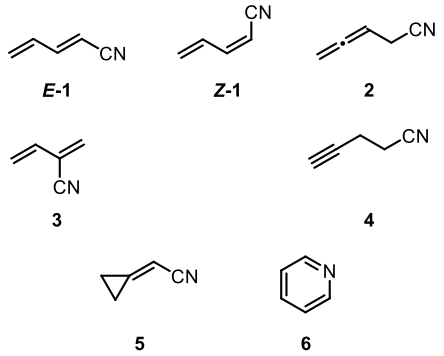

Figure 1. C_5H_5N isomers studied by rotational spectroscopy: (*E*)-1-cyano-1,3-butadiene (***E*-1**), (*Z*)-1-cyano-1,3-butadiene (***Z*-1**), 4-cyano-1,2-butadiene (**2**), 2-cyano-1,3-butadiene (**3**), 4-cyano-1-butyne (**4**), (cyanomethylene)cyclopropane (**5**), and pyridine (**6**).

Received: April 10, 2021
Revised: May 28, 2021
Published: June 21, 2021

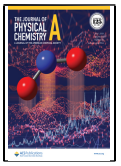

environments.[16−18] Expanding the family of pyridine isomers facilitates future investigations of the reactivity of these small molecules and astronomical searches for these species in extraterrestrial environments. Astronomical detections of any of the molecules from either group would be of fundamental interest and could illuminate new astrochemical pathways toward complex aromatic species.

(Cyanomethylene)cyclopropane (**5**) (2-cyclopropylideneacetonitrile) is a structurally intriguing molecule (Figure 2).

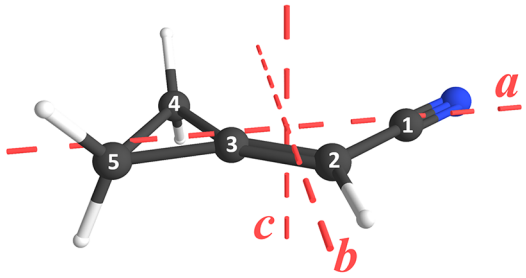

Figure 2. (Cyanomethylene)cyclopropane (**5**) (C_s, C_5H_5N) structure with principal inertial axes (μ_a = 4.4 D, μ_b = 1.2 D).

It is substantially higher in energy than its isomer, pyridine [*ca.* 50 kcal/mol, B3LYP/6-311+G(2d,p)] due to the absence of aromaticity and the presence of a strained, three-membered cyclopropyl ring with the exocyclic π bond. The inherent strain energy of three-membered rings notwithstanding, four interstellar molecules include this structural motif (with differing degrees of unsaturation): cyclopropenylidene (*c*-C_3H_2),[19] cyclopropenone (C_3H_2O),[20] ethylene oxide (*c*-C_2H_4O),[21] and propylene oxide ($CH_3C_2H_3O$).[22] Additionally, **5** contains an α,β-unsaturated nitrile moiety, which is similar to the known interstellar species vinyl cyanide ($H_2C{=}CHCN$; acrylonitrile),[23] cyanoallene ($H_2C{=}C{=}CHCN$),[24] and methylcyano-acetylene ($CH_3C{\equiv}CCN$).[25] The role of (cyanomethylene)cyclopropane (**5**) in the chemical mechanisms of formation or destruction of pyridine (**6**) remains a matter of conjecture, but we are continuing our investigations of the reaction chemistry of **5** under a variety of harsh conditions.

(Cyanomethylene)cyclopropane (**5**) is an attractive candidate for astronomical search, being a nitrile-containing structural isomer of pyridine (C_s, C_5H_5N) and a highly prolate, asymmetric top (κ = −0.96) with a strong dipole [μ_a = 4.4 D, μ_b = 1.2 D, MP2/6-311+G(2d,p)]. This molecule has been generated only twice previously,[19,20] and the characterization data are quite limited compared to other simple organic nitriles. As shown in Scheme 1a, Wilson first generated **5** in

Scheme 1. Previous Syntheses of (Cyanomethylene)cyclopropane (5)[a]

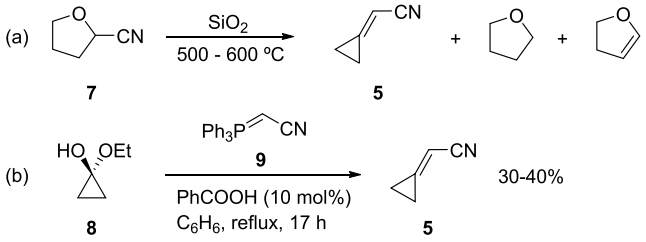

[a]Yield estimated by NMR.

1945 by pyrolysis of 2-cyanotetrahydrofuran (**7**) at 500−600 °C on silica with coproduction of tetrahydrofuran and dihydrofuran.[26] While effective at generating the desired compound, it is not an ideal synthetic approach for studying its rotational spectrum due to the generation of volatile byproducts with permanent dipole moments as sample contaminants. More recently, Mauduit *et al.* reported a facile, gram-scale synthesis of **5** *via* a Wittig reaction of 1-ethoxycyclopropanol (**8**) with (cyanomethylene)-triphenylphosphorane (**9**) (Scheme 1b).[27] This synthesis is ideal for analysis by rotational spectroscopy as it produces the desired product in significant quantity without volatile, polar solvents or byproducts. A slightly modified version of this synthetic procedure, along with improved procedures for isolation of **5**, provided the foundation of this spectroscopic investigation.

EXPERIMENTAL AND THEORETICAL METHODS

Synthesis. Our synthetic approach to (cyanomethylene)-cyclopropane (**5**) is based upon previous work of Mauduit *et al.*[27] as shown in Scheme 1b. The desired compound was obtained in three relatively simple steps with sufficient quantity and purity to enable the spectroscopic investigation (Scheme 2). A commercial sample of (1-ethoxycyclopropoxy)-

Scheme 2. Modified Synthesis of (Cyanomethylene)cyclopropane (5)[a]

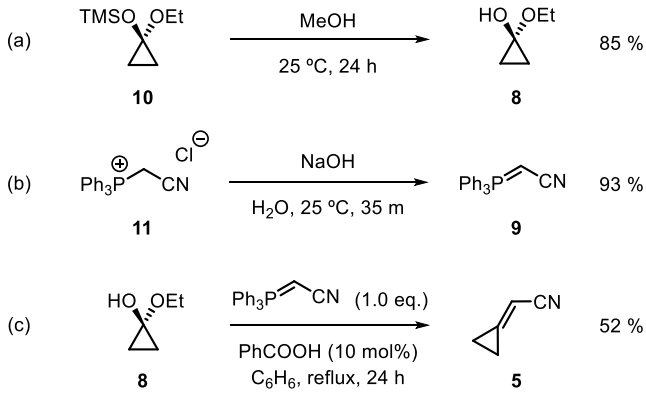

[a]Isolated yields.

trimethylsilane (**10**) was deprotected by stirring in methanol for 24 h to reveal the required hemiketal **8** in 85% yield.[28] Ylide **9** was prepared in 93% yield from a commercial sample of (cyanomethyl)triphenylphosphonium chloride (**11**) by stirring in basic solution for 35 min. Subsequently, **8** and **9** were allowed to react in refluxing benzene with catalytic benzoic acid to generate (cyanomethylene)cyclopropane (**5**), which was isolated as a pure substance, for the first time, in 52% yield. As previously reported,[27] this reaction could be carried out in a variety of nonpolar organic solvents. Benzene was selected, in this case, because it does not possess a permanent dipole moment, and any residual benzene would not be observed in the rotational spectrum. After distillation, this sample was used to measure the rotational spectrum of (cyanomethylene)cyclopropane (**5**). Detailed experimental procedures and characterization data are provided below for each compound.

Spectroscopy. Using a millimeter-wave spectrometer that has been previously described,[29,30] the rotational spectrum of

https://doi.org/10.1021/acs.jpca.1c03246
J. Phys. Chem. A 2021, 125, 5601−5614

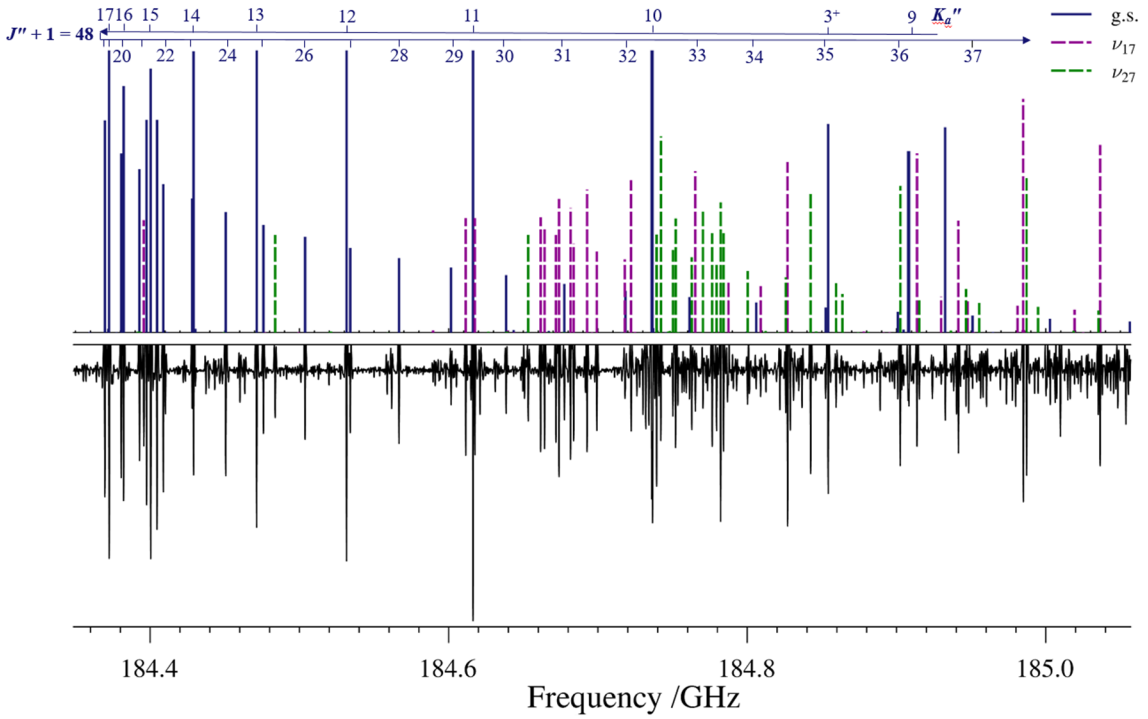

Figure 3. Predicted (top) and experimental (bottom) rotational spectrum of (cyanomethylene)cyclopropane (**5**) from 184.35 to 185.05 GHz. Ground-state transitions for the $J'' + 1 = 48$ band in dark blue, ν_{17} in purple, and ν_{27} in green.

(cyanomethylene)cyclopropane (**5**) was collected from 130 to 230 and from 235 to 360 GHz in a continuous flow at room temperature with a sample pressure of 4 mTorr. The separate spectral segments were combined into a single broadband spectrum using Kisiel's Assignment and Analysis of Broadband Spectra software.[31,32] Pickett's SPFIT/SPCAT[33] and Kisiel's ASFIT/ASROT[31,32] were used for least-squares fits and spectral predictions, along with the PIFORM, PMIXC, PLANM, and AC programs for analysis.[34] A uniform frequency measurement uncertainty of 0.050 MHz was assumed for all measurements.

Computation. Electronic structure calculations were carried out with Gaussian 16[35] using the WebMO interface[36] to obtain theoretical spectroscopic constants. Optimized geometries at the B3LYP/6-311+(2d,p) and MP2/6-311+(2d,p) levels were obtained using "verytight" convergence criteria and an "ultrafine" integration grid, and subsequent anharmonic vibrational frequency calculations were carried out. The B3LYP predictions of the spectroscopic constants, which were sufficient to begin the analysis, did not have the expected agreement with the experimental spectroscopic constants. Thus, MP2 calculations were performed which had slightly closer agreement with the experimental constants. All computational output files can be found in the Supporting Information.

RESULTS AND DISCUSSION

Ground Vibrational State. (Cyanomethylene)-cyclopropane (**5**) is a highly prolate, asymmetric top molecule ($\kappa = -0.96$) with strong dipole moments along its *a*- and *b*-principal axes ($\mu_a = 4.4$ D, $\mu_b = 1.2$ D, MP2). As shown in Figure 3, its rotational spectrum in the 130 to 360 GHz region is dominated by intense $^aR_{0,1}$ transitions that appear in clearly observable bands of transitions sharing a single J value. At low values of K_a, the plus- and minus-symmetry $^aR_{0,1}$ transitions are nondegenerate and located far from these obvious bands. As the K_a value increases, the plus- and minus-symmetry transitions become degenerate and progress to lower frequency before experiencing a turnaround and forming the recognizable bandhead. As expected for the spectrum of a highly prolate molecule, these bands are separated by approximately $B + C$ (~3.8 GHz). The transitions progress to higher frequency away from the bandhead with further increasing K_a until the transitions are lost in the spectral confusion limit. Much lower intensity *b*-type ($^bR_{1,1}$ and $^bR_{-1,1}$) transitions are observable with low values of K_a, some of which become degenerate with the much more intense $^aR_{0,1}$ transitions in this frequency range. Transitions from 11 $^bQ_{1,-1}$ branch series with constant K_a are also visible across our observed frequency range. They increase in J and intensity as they progress to higher frequency, forming an identifiable band structure, turn around, and progress to lower frequency with further increasing J. Eventually, the degenerate transitions separate to form pairs of plus- and minus-symmetry $^bQ_{1,-1}$ transitions. Finally, a limited number of low-intensity, degenerate $^bP_{1,-1}$ and $^bP_{1,-3}$ transitions are also included in the data set. Due to the relatively high values of J and K for the transitions observed in this work, nuclear quadrupole splitting was not resolved and thus not treated in the data analysis.

Due to the high spectral density shown in Figure 3, the detection limit for transitions of all species in the observed spectrum is due to spectral confusion, rather than the signal-to-noise ratio. Because this sample was prepared by an intentional synthesis, purified by vacuum distillation, and characterized by other spectroscopic techniques (MS and NMR), we are confident that the vast majority of the spectral features are from **5** and not an impurity. The ground and vibrationally excited states of **5** each contribute a few thousand transitions to the rotational spectrum from 130 to 360 GHz. This spectral density makes accurate measurement of low-intensity tran-

https://doi.org/10.1021/acs.jpca.1c03246
J. Phys. Chem. A 2021, 125, 5601−5614

Table 1. Spectroscopic Constants for the Ground Vibrational State of (Cyanomethylene)cyclopropane (5) (S- and A-Reduced Hamiltonian, I^r Representation)[e]

	S Reduction, I^r representation			A Reduction, I^r representation	
	Experimental	MP2 [a]		Experimental	MP2 [a]
A_0 (MHz)	12644.00265 (20)	12527	A_0 (MHz)	12644.00216 (20)	12527
B_0 (MHz)	2038.861622 (59)	2014	B_0 (MHz)	2038.866459 (58)	2014
C_0 (MHz)	1797.034263 (54)	1776	C_0 (MHz)	1797.029487 (53)	1776
D_J (kHz)	0.561813 (18)	0.540	Δ_J (kHz)	0.575343 (17)	0.552
D_{JK} (kHz)	−7.547487 (70)	−7.43	Δ_{JK} (kHz)	−7.629007 (69)	−7.51
D_K (kHz)	63.1448 (11)	63.1	Δ_K (kHz)	63.2116 (10)	63.2
d_1 (kHz)	−0.1207251 (70)	−0.115	δ_J (kHz)	0.1207298 (69)	0.115
d_2 (kHz)	−0.00676037 (56)	−0.00618	δ_K (kHz)	2.40341 (20)	2.25
H_J (Hz)	0.0009849 (25)	0.000857	Φ_J (Hz)	0.0010541 (25)	0.000913
H_{JK} (Hz)	−0.020207 (12)	−0.0184	Φ_{JK} (Hz)	−0.012678 (39)	−0.0117
H_{KJ} (Hz)	0.052221 (75)	0.0364	Φ_{KJ} (Hz)	0.02518 (15)	0.0130
H_K (Hz)	0.6080 (19)	0.686	Φ_K (Hz)	0.6261 (18)	0.702
h_1 (Hz)	0.0003513 (12)	0.000304	ϕ_J (Hz)	0.0003565 (11)	0.000309
h_2 (Hz)	0.000033184 (83)	0.0000279	ϕ_{JK} (Hz)	0.005722 (30)	0.00418
h_3 (Hz)	0.000005436 (25)	0.00000487	ϕ_K (Hz)	0.4541 (22)	0.413
L_J (μHz)	−0.00200 (12)		L_J (μHz)	−0.00220 (11)	
L_{JJK} (μHz)	0.07038 (76)		L_{JJK} (μHz)	0.05070 (75)	
L_{JK} (μHz)	−1.1331 (47)		L_{JK} (μHz)	1.2714 (46)	
L_{KKJ} (μHz)	−2.134 (31)		L_{KKJ} (μHz)	−1.169 (32)	
L_K (μHz)	[0.0]		L_K (μHz)	[0.0]	
l_1 (μHz)	−0.000984 (64)		l_J (μHz)	−0.000978 (63)	
l_2 (μHz)	[0.0]		l_{JK} (μHz)	[0.0]	
l_3 (μHz)	[0.0]		l_{KJ} (μHz)	[0.0]	
l_4 (μHz)	[0.0]		l_K (μHz)	[0.0]	
Δ_i (uÅ^2) [b,c]	−6.613509 (11)	−6.716	Δ_i (uÅ^2) [b,c]	−6.612175 (11)	−6.716
N_{lines} [d]	3933		N_{lines} [d]	3933	
σ_{fit} (MHz)	0.031		σ_{fit} (MHz)	0.031	

[a]Evaluated with the 6-311+G(2d,p) basis set. [b]Inertial defect, $\Delta_i = I_c - I_a - I_b$. [c]Calculated using PLANM from the B_0 constants. [d]Number of fitted transition frequencies. [e]Values in square brackets held fixed in least-squares fit.

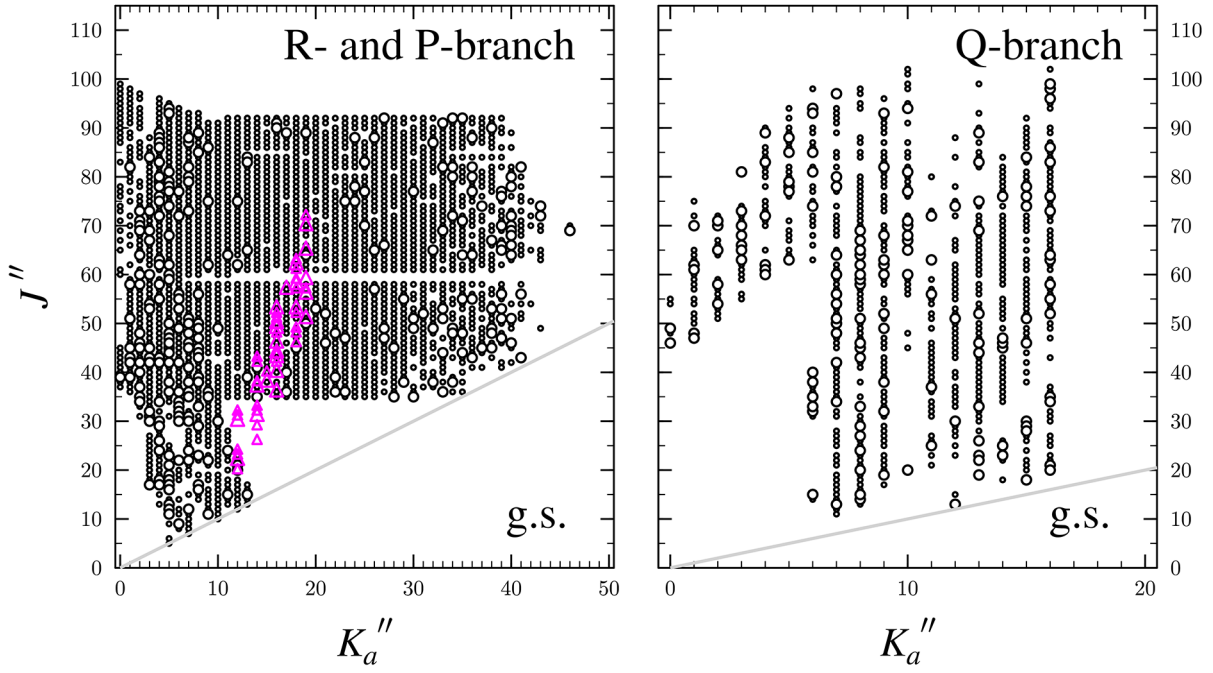

Figure 4. Data distribution plots for the least-squares fit of spectroscopic data for the vibrational ground state of (cyanomethylene)cyclopropane (**5**). R-branch and Q-branch transitions are represented by black circles. P-branch transitions are represented as pink triangles. The size of the symbol is proportional to the value of $|(f_{obs.} - f_{calc.})/\delta f|$, where δf is the frequency measurement uncertainty.

https://doi.org/10.1021/acs.jpca.1c03246
J. Phys. Chem. A 2021, 125, 5601−5614

sitions challenging due to coincidental overlapping transitions from other vibrational states. It also makes observation of the [^{13}C]- or [^{15}N]-isotopologues at their natural abundances particularly difficult, as there are a few dozen vibrationally excited states with transitions of higher intensity. Using standard methods of predicting the spectra of these isotopologues from the spectroscopic constants of the main isotopologue and computed constants for the main and heavy atom isotopologues, none of these species were observable in the experimental spectrum. Thus, the spectral analysis presented in this work is limited to the ground and two lowest-energy vibrationally excited states.

A total of over 3900 ground-state transitions were observed, measured, and least-squares fit to partial octic, distorted rotor A- and S-reduced Hamiltonians in the I^r representation (σ_{fit} = 0.031 MHz). The resulting values of the spectroscopic constants and their theoretical counterparts are provided in Table 1. The MP2 predictions of the rotational constants are within about 1% of their experimentally determined values. The B3LYP values provided in Table S1 are in slightly worse agreement, with errors in B_0 and C_0 of 1.9 and 1.6%, respectively. While these predictions are quite reasonable and of the expected quality, the absolute error in the predicted spectrum resulting from them is substantial. As mentioned, the most recognizable features of the rotational spectrum are the $^aR_{0,1}$ bands ranging from J = 35 to 93 across the observed frequency range. With these bands separated by approximately $B + C$ and the sum of these constants predicted to be too small (66 MHz with B3LYP and 46 MHz with MP2), the initial predictions of each band's location were off by 2.3−6.1 GHz (B3LYP) and 1.6−4.3 GHz (MP2). The large relative errors of the computed $B + C$ compared to the experimental value of 3835.895885 (80) MHz, however, did not substantially hinder the assignment of transitions.

The large number of measured transition and the diversity of J (5 to 102) and K_a (0 to 46) values in the data set (Figure 4) enabled the quartic and sextic centrifugal distortion constants to be very well determined. The experimental quartic centrifugal distortion constants should be very reliable, given the inclusion of a full set of sextic centrifugal distortion constants. For both reductions, the MP2 quartic centrifugal distortion constants are within 9% of their experimental values. In particular, there is remarkable agreement for the D_K and Δ_K constants, where the predicted values are nearly identical to the experimental values. Both values are quite large (>60 kHz) due to the very prolate (κ = −0.96) nature of **5**, which is consistent with other highly prolate species.[29,37] Due, in part, to the incomplete set of octic centrifugal distortion terms included in the Hamiltonian, the determination of the sextic centrifugal distortion terms is less reliable. All MP2 values of the constants are of the correct sign and magnitude, though some differ by as much as 50% from their experimental values. No method is currently implemented in Gaussian (or other commonly available computational software) for estimating the octic centrifugal distortion constants, so no comparison can be made between experiment and theory. This absence of a prediction also reduces the physical meaningfulness of those parameters that are varied in the least-squares fit, as remaining constants that cannot be satisfactorily determined cannot be held constant at a theoretical value and must instead be held constant at zero. Nevertheless, it appears that the centrifugal distortion constants for the ground state are sufficiently well determined (particularly the octic and sextic ones) that they can be used with confidence for any distortion constants of the vibrationally excited states that cannot be determined in their least-squares fits.

Fundamental Vibrational States ν_{27} and ν_{17}. The vibrationally excited states of (cyanomethylene)cyclopropane (**5**) below 500 cm^{-1} consist of a Coriolis-coupled dyad of its two lowest-energy fundamentals and a complex polyad of several higher-energy vibrationally excited states (Figure 5).

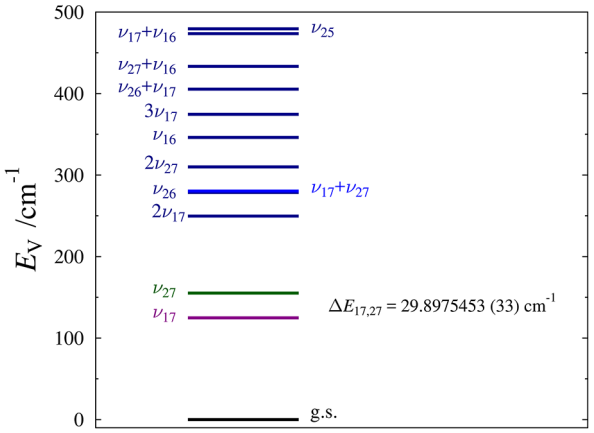

Figure 5. Vibrational energy levels of (cyanomethylene)cyclopropane (**5**) below 500 cm^{-1} from the computed fundamental frequencies (MP2/6-311+G(2d,p)). The value of $\Delta E_{17,27}$ results from the experimental perturbation analysis of ν_{17} and ν_{27} in this work.

The lowest-energy fundamental, ν_{17} (A', 125 cm^{-1}), is an in-plane bend of the nitrile and cyclopropyl groups with respect to C2 and C3. The second-lowest energy fundamental, ν_{27} (A'', 155 cm^{-1}), is a symmetric, out-of-plane bend of the nitrile and a CH_2 of the cyclopropyl with respect to the ethylene. The two lowest-energy fundamentals are expected to show strong interactions between their energy levels due to the large values of A_ν, their moderate predicted energy difference of 30 cm^{-1} (MP2), the large predicted Coriolis ζ values, and the range of J values observed in this work. As expected, the transitions of these vibrationally excited states are not adequately treated by single-state, distorted-rotor Hamiltonians. A two-state partial octic, A-reduced Hamiltonian with nine terms treating the coupling between states was used to successfully least-squares fit the transitions for the ν_{17} and ν_{27} dyad. The final data set includes over 2600 transitions for each fundamental state and is least-squares fit to a low statistical error (σ_{fit} < 0.039 MHz). As shown in Figure 6, the range of J (6 to 99) and K_a (0 to 37) values represented is still quite extensive, albeit reduced from the ground-state data set. Due to the lower intensity of these two vibrationally excited states, substantially fewer Q-branch transitions could be measured and included in the least-squares fit. No P-branch transitions could be measured or included for these lower-intensity states.

The resulting spectroscopic constants for ν_{17} and ν_{27} (Table 2) include a complete set of well-determined rotational and quartic centrifugal distortion constants. The least well-determined rotational constants, A_{17} and A_{27}, have statistical uncertainties of about 0.01% the magnitude of their values. The A_ν constants are hardest to determine for a molecule such as (cyanomethylene)cyclopropane (**5**), given that the majority of observed transitions are a-type and relatively few are b-type. This is true for the ground state as well as the excited

https://doi.org/10.1021/acs.jpca.1c03246
J. Phys. Chem. A 2021, 125, 5601−5614

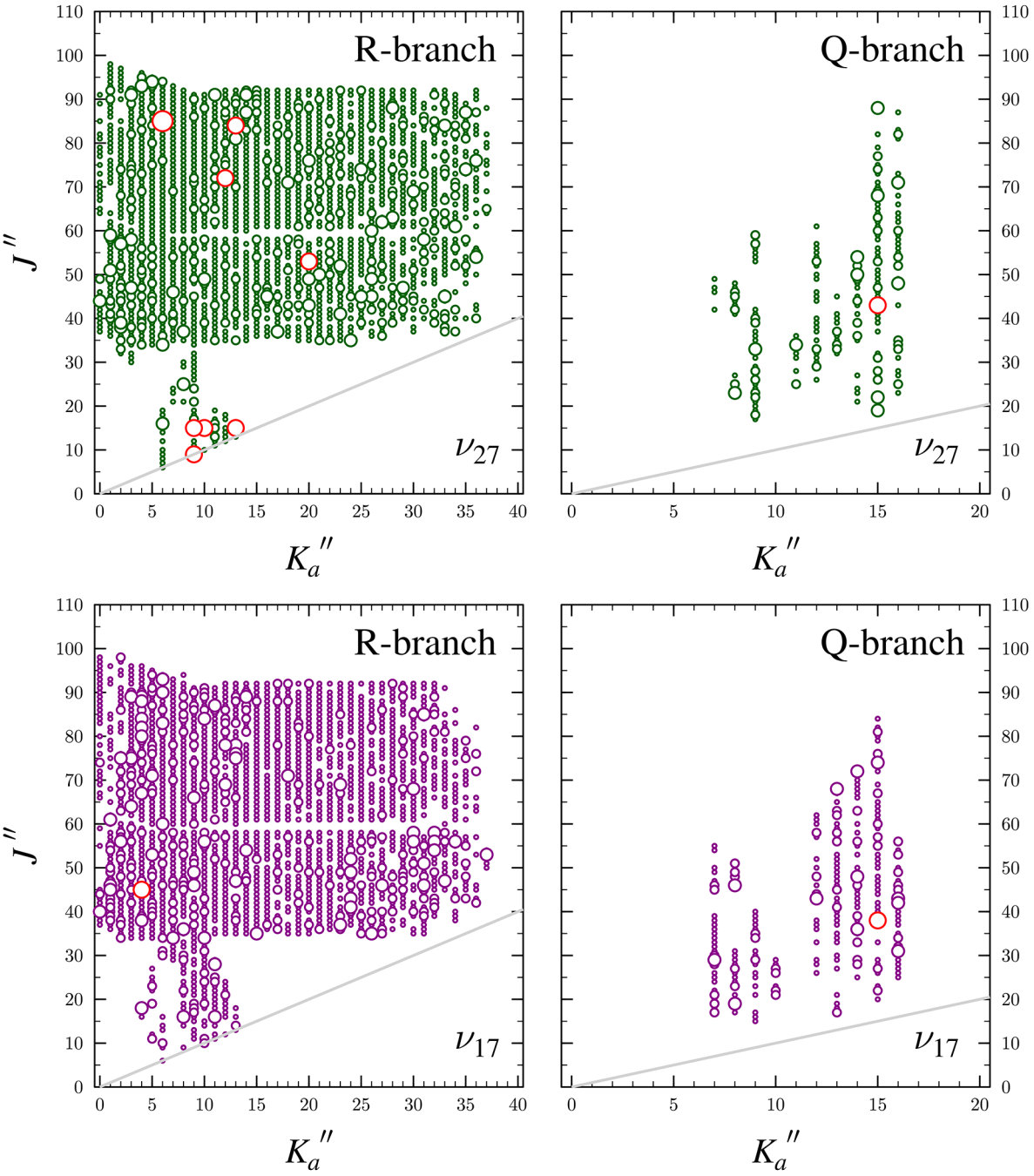

Figure 6. Data distribution plots for the coupled fit of measured transitions in the two lowest-energy excited vibrational states in (cyanomethylene)cyclopropane (**5**). The size of the plotted symbol is proportional to the value of $|(f_{obs.} - f_{calc.})/\delta f|$, where δf is the frequency measurement uncertainty (50 kHz). Values for which this relative error is >3 shown in red.

vibrational states. Even more problematic, the *Av* constants are also the most correlated with the large *a*-type Coriolis-coupling constants and are therefore generally more poorly determined in the fit of a coupled dyad. Only a few *J*-dependent sextic constants (Φ_J Φ_{JK}, and ϕ_J) could be determined, and all other centrifugal distortion constants were held constant at their ground-state values. With no method currently implemented to obtain theoretical values for the quartic distortion constants of these fundamentals, only a comparison to their ground-state counterparts is possible. With a complete set of quartic distortion constants, but only an incomplete set of sextic distortion constants, the quartic distortion constants provide the more reliable estimation of how well the least-squares fit is treating the perturbations between ν_{17} and ν_{27}. The relatively small deviations (<10%) of all quartic constants from their ground-state counterparts suggest that the coupling is being sufficiently treated and that these values are physically meaningful. None of these constants bears a clear sign of absorbing untreated coupling between the states, which would typically cause large deviations in some spectroscopic constants in opposite directions relative to the ground-state constants.

https://doi.org/10.1021/acs.jpca.1c03246
J. Phys. Chem. A 2021, 125, 5601−5614

Table 2. Spectroscopic Constants for Vibrationally Excited States ν_{17} and ν_{27} of (Cyanomethylene)cyclopropane (5) (A-Reduced Hamiltonian, I^r Representation)[e]

	Ground state	ν_{17} (A', 125 cm^{-1}) [a]	ν_{27} (A', 155 cm^{-1}) [a]
A_v (MHz)	12644.00216 (20)	12725.8 (12)	12570.5 (12)
B_v (MHz)	2038.866459 (58)	2044.336 (18)	2041.600 (18)
C_v (MHz)	1797.029487 (53)	1799.526614 (64)	1800.078788 (50)
Δ_J (kHz)	0.575343 (17)	0.577820 (28)	0.578479 (28)
Δ_{JK} (kHz)	−7.629007 (69)	−7.6499 (17)	−7.5923 (17)
Δ_K (kHz)	63.2116 (10)	63.021 (32)	63.649 (32)
δ_J (kHz)	0.1207298 (69)	0.122045 (15)	0.121117 (15)
δ_K (kHz)	2.40341 (20)	2.6318 (11)	2.3490 (10)
Φ_J (Hz)	0.0010541 (25)	0.00103342 (48)	0.00107110 (49)
Φ_{JK} (Hz)	−0.012678 (39)	−0.013792 (83)	−0.010726 (84)
Φ_{KJ} (Hz)	0.02518 (15)	[0.02518]	[0.02518]
Φ_K (Hz)	0.6261 (18)	[0.6261]	[0.6261]
ϕ_J (Hz)	0.0003565 (11)	0.00034856 (48)	0.00036235 (42)
ϕ_{JK} (Hz)	0.005722 (30)	[0.005722]	[0.005722]
ϕ_K (Hz)	0.4541 (22)	[0.4541]	[0.4541]
ΔE		896305.858 (98) MHz / 29.8975453 (33) cm^{-1}	
G_a (MHz)		16023. (32)	
G_a^J (MHz)		0.012739 (88)	
G_a^K (MHz)		−0.3961 (60)	
G_a^{JJ} (MHz)		−0.0000000919 (20)	
F_{bc} (MHz)		0.6737 (19)	
F_{bc}^J (MHz)		−0.000000374 (19)	
F_{bc}^K (MHz)		0.00034376 (81)	
G_b (MHz)		1371.4 (59)	
G_b^J (MHz)		−0.002270 (25)	
Δ_i (uÅ^2) [b,c]	−6.613509 (11)	−6.06823 (43)	−6.9904 (44)
N_{lines} [d]	3933	2789	2666
σ_{fit} (MHz)	0.031	0.038	0.039

[a]Fundamental frequencies calculated using MP2/6-311+G(2d,p). [b]Inertial defect, $\Delta_i = I_c - I_a - I_b$. [c]Calculated using PLANM from the B_0 constants. [d]Number of fitted transition frequencies. [e]Values in square brackets held fixed in least-squares fit.

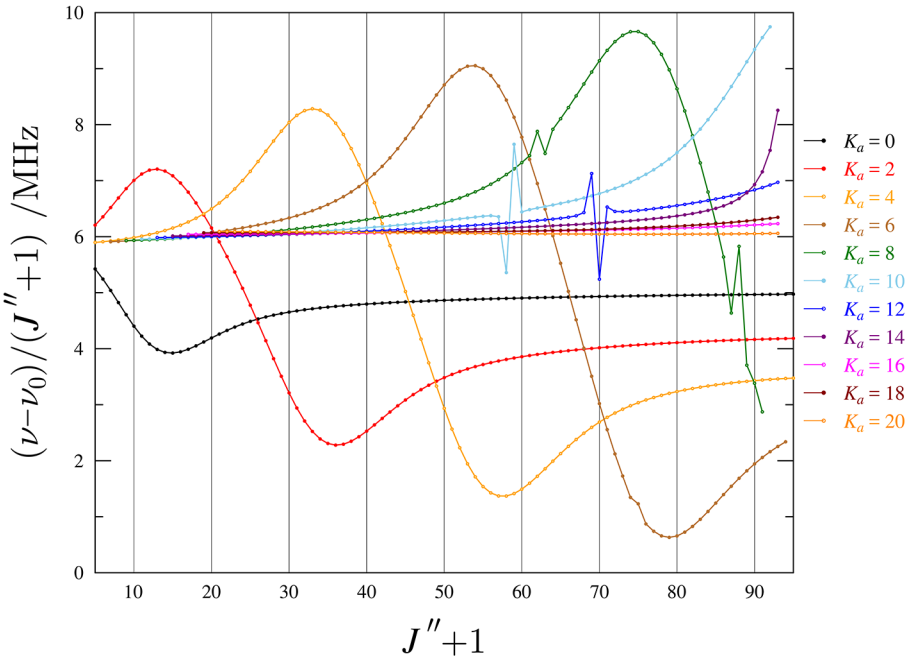

Figure 7. Superimposed resonance plots of ν_{17} for $^aR_{0,1}$ K_a^+ series with even values of K_a^+ between 0 and 30 for (cyanomethylene)cyclopropane (**5**). Measured transitions are omitted for clarity, but they are indistinguishable from the plotted values on this scale. The plotted values are frequency differences between excited-state transitions and their ground-state counterparts, scaled by (J'' + 1).

https://doi.org/10.1021/acs.jpca.1c03246
J. Phys. Chem. A 2021, 125, 5601−5614

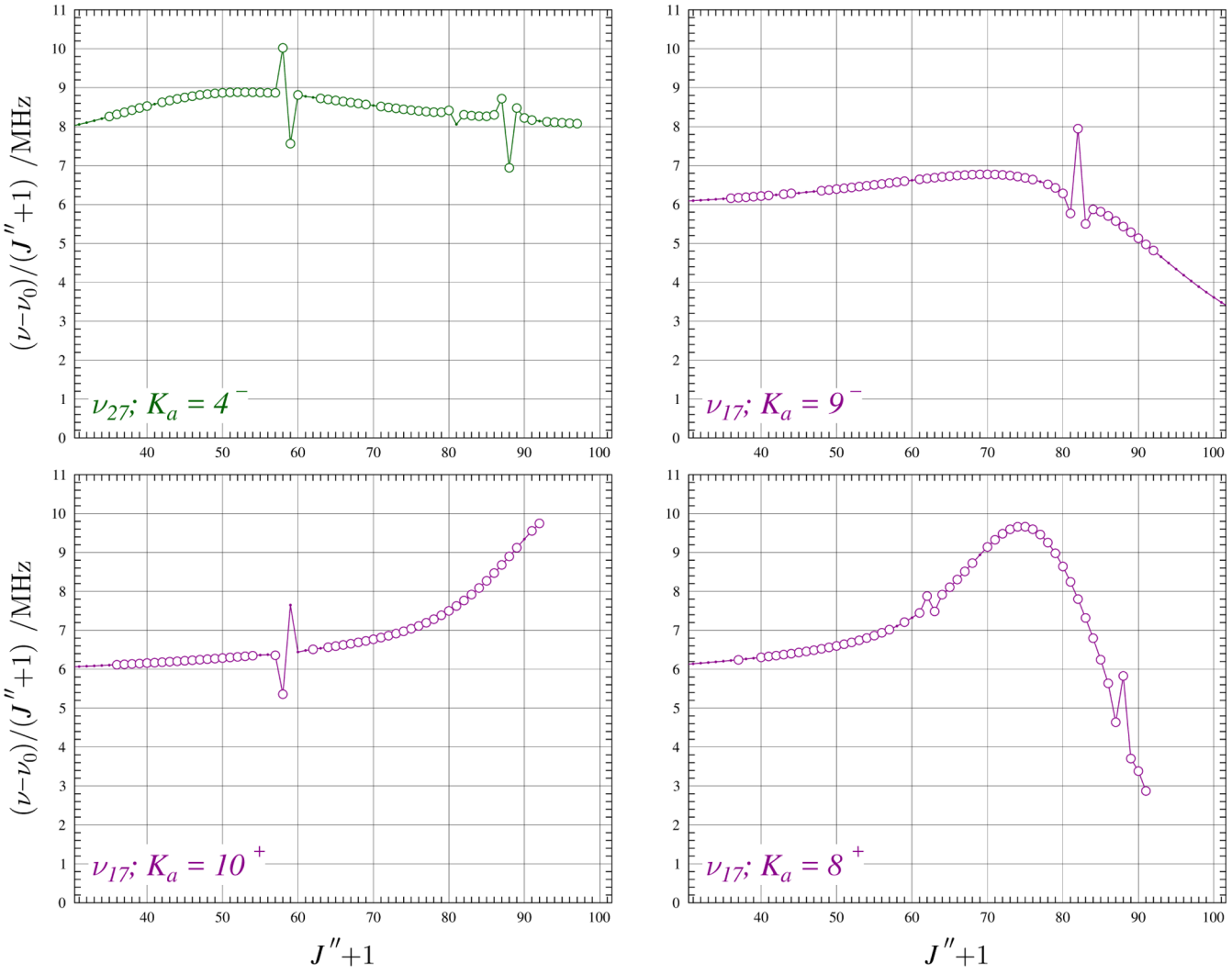

Figure 8. Resonance plots for (cyanomethylene)cyclopropane (**5**) showing the $K_a = 4^-$ series for ν_{27} and $K_a = 9^-$, 10^+, and 8^+ series for ν_{17}. Examples of resonances conforming to the $\Delta K_a = 5$ and $\Delta K_a = 6$, 4 selection rules for *b*- and *a*-type resonances, respectively. The plotted values are frequency differences between excited-state transitions and their ground-state counterparts, scaled by $(J'' + 1)$ in order to make the plots more horizontal. Measured transitions are represented by circles: ν_{17} (purple); ν_{27} (green). There are no measured transitions with $|(f_{obs.} - f_{calc.})/\delta f| > 3$. Predictions from the final coupled fit are represented by a solid, colored line.

Coriolis-Coupling Analysis. The satisfactory treatment and least-squares fitting of the coupled dyad between ν_{17} and ν_{27} provide a highly precise and accurate energy difference [$\Delta E_{17,27}$ = 896305.858 (98) MHz or 29.8975453 (33) cm^{-1}] between these fundamentals. Both the MP2 (30.4 cm^{-1}) and B3LYP (29.5 cm^{-1}) energy differences are in unexpectedly close agreement with the experimentally determined value. The precision of the experimentally determined energy difference is dependent upon the inclusion of many transitions involved in global interactions between the fundamentals, transitions whose energy levels are impacted by energy level crossings (causing sharp local resonances), and related formally forbidden interstate transitions. The energy difference is very sensitive to, and well-determined by, the last two kinds of frequency data.

In the initial fitting process, the global perturbations between states can be seen as the undulations or curvature of the resonance plots for the K_a series of R-branch transitions. Several example series are shown in Figures 7 and 8 for ν_{17} and ν_{27}. As the quantum number value of K_a increases, the peak and trough of the undulation progress rapidly toward higher J values. By K_a = 12 for ν_{17}, the undulations of the series have largely passed out of the observed range of J, and the K_a series appear to be much flatter. These curving series of ν_{17}, combined with the mirrored undulations in the resonance plots of the low-K_a series of ν_{27}, allow for an initial fitting and refinement of the Coriolis-coupling terms and $\Delta E_{17,27}$. Once there is a preliminary treatment of the global interaction, the local resonances (Figures 7 and 8) can be assigned and included in the least-squares fit data set. These intense interactions become visibly noticeable at $K_a \sim 6$ for ν_{17} (lower K_a for ν_{27}) and provide critical refinement of the energy and coupling coefficients. Eventually, these global undulations and local resonances allow for a precise determination of the Coriolis-coupling coefficients and $\Delta E_{17,27}$ and should result in rotational and centrifugal distortion constants that are relatively free of the impact of untreated coupling between states.

The different symmetries of fundamentals ν_{17} (A', 125 cm^{-1}) and ν_{27} (A'', 155 cm^{-1}) permit Coriolis couplings along both their *a*- and *b*-principal axes. Both of the resulting types of *a*- and *b*-type resonances (ΔK_a = even and ΔK_a = odd,

https://doi.org/10.1021/acs.jpca.1c03246
J. Phys. Chem. A 2021, 125, 5601−5614

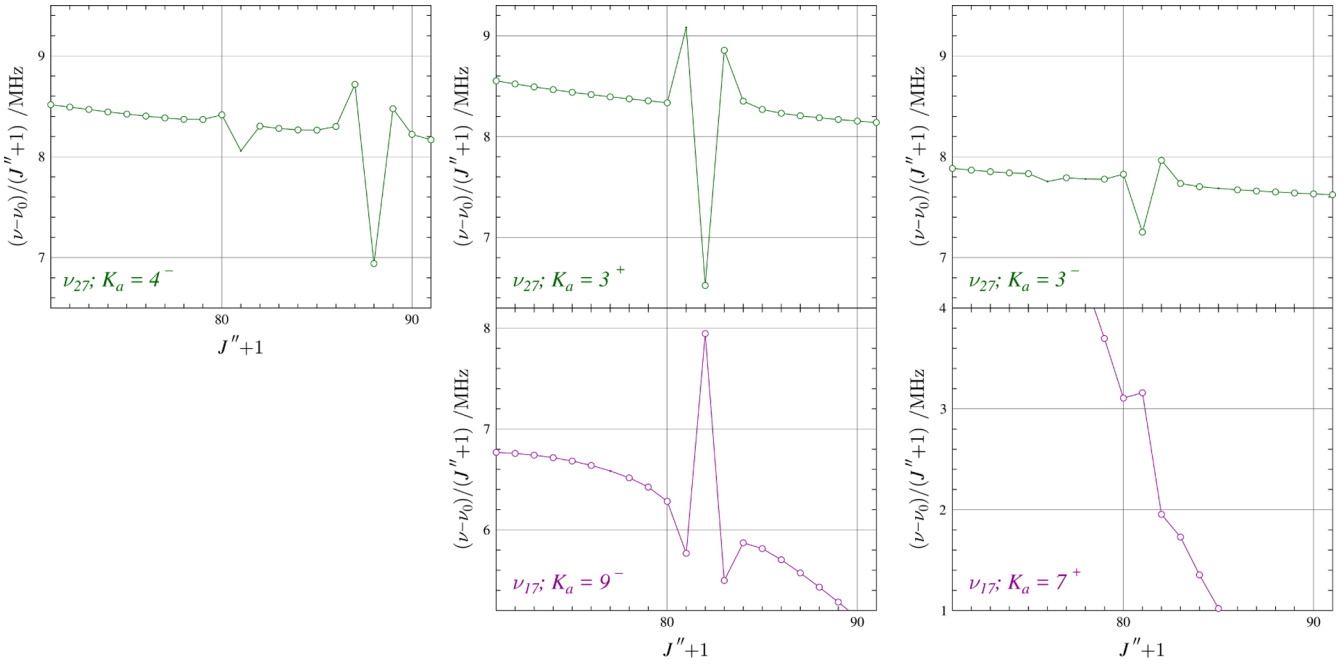

Figure 9. Resonance plots for (cyanomethylene)cyclopropane (**5**) showing the $K_a = 4^-$, 3^+, and 3^- series for ν_{27} and the $K_a = 9^-$ and 7^+ series for ν_{17}. All of these series have transitions affected by perturbation at $J'' + 1 = 81$. The plotted values are frequency differences between excited-state transitions and their ground-state counterparts, scaled by $(J'' + 1)$ in order to make the plots more horizontal. Measured transitions are represented by circles: ν_{17} (purple); ν_{27} (green). There are no measured transitions with $|(f_{obs.} - f_{calc.})/\delta f| > 3$. Predictions from the final coupled fit are represented by a solid, colored line.

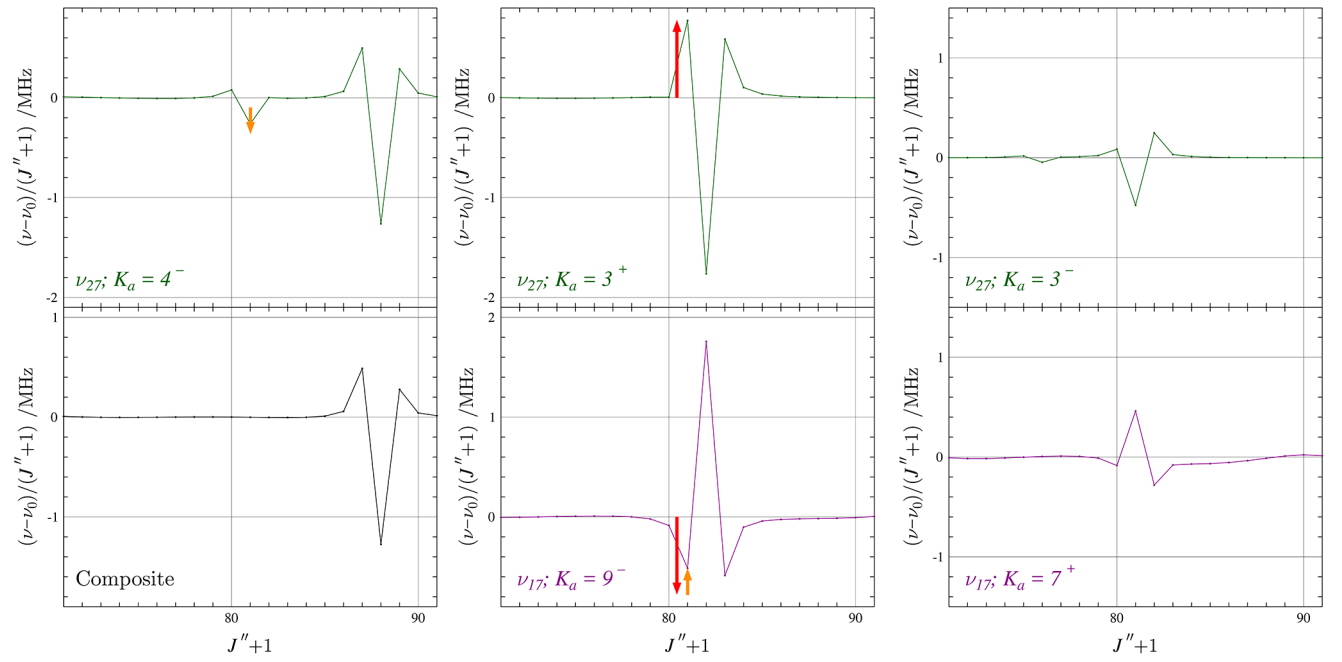

Figure 10. Baseline-flattened resonance plots for (cyanomethylene)cyclopropane (**5**) showing the $K_a = 4^-$, 3^+, and 3^- series for ν_{27} and the $K_a = 9^-$ and 7^+ series for ν_{17}, as well as a composite plot of ν_{27} $K_a = 4^-$, ν_{27} $K_a = 3^+$, and ν_{17} $K_a = 9^-$. All of these series have transitions affected by perturbation at $J'' + 1 = 81$. Measured transitions are omitted for clarity, but they are indistinguishable from the plotted values on this scale. Red arrows denote the magnitude of frequency displacement due to the *a*-type interaction between transitions of ν_{27} $K_a = 3^+$ and ν_{17} $K_a = 9^-$ at $J'' + 1 = 81$, and orange arrows denote the magnitude of frequency displacement due to the *b*-type interaction between transitions of ν_{27} $K_a = 4^-$ and ν_{17} $K_a = 9^-$ at $J'' + 1 = 81$.

respectively) are observed between ν_{17} and ν_{27}. An informative example is shown in Figure 7, involving resonances between the $K_a = 4^-$ series of ν_{27} and the $K_a = 9^-$, 10^+, and 8^+ series of ν_{17}. These resonances showcase the two possible appearances of resonances, with either a single highly displaced transition or with two highly displaced transitions in opposite directions. The former occurs when the energy crossing of the vibrational states occurs at or very near to a single J quantum number. The

https://doi.org/10.1021/acs.jpca.1c03246
J. Phys. Chem. A 2021, 125, 5601−5614

latter occurs when the exact energy level crossing of the vibrational states occurs midway between two different J quantum numbers. The first of the three small resonances (J'' + 1 = 58, 59) in the $K_a = 4^-$ series of ν_{27} is the result of an a-type interaction with the $K_a = 10^+$ series of ν_{27} ($\Delta K_a = 6$). Due to both of these resonances occurring at relatively flat regions of the curving series, the mirroring of these resonances is visually apparent with both plots using the same y-axis scale. The absent resonant transition of the ν_{27} series is excluded due to its near-degeneracy with a $K_a = 2$ transition from the ground state, preventing an accurate measurement of either transition. The second of the three small resonances (J'' + 1 = 81) is the result of a complicated interaction with the $K_a = 9^-$ series of ν_{17} ($\Delta K_a = 5$) (*vide infra*). The ν_{27} transition of this resonance is not included in the data set due to a significant loss of intensity to its related nominal interstate transition, combined with an incidental overlap with two significantly more intense transitions. The final resonance (J'' + 1 = 88) is due to a second a-type interaction with the $K_a = 8^+$ series of ν_{17} (ΔK_a = 4). The $K_a = 8^+$ series of ν_{17} has a second small resonance (J'' + 1 = 62, 63) with the $K_a = 2^-$ series (resonance plot not shown) of ν_{27} ($\Delta K_a = 6$).

It is not readily apparent from Figure 8 that the ν_{27} transition at J'' + 1 = 81 is involved in a b-type, $\Delta K_a = 5$ interaction with a transition in the $K_a = 9^-$ series of ν_{17} because these two features appear quite unsymmetrical. It so happens that five different K_a series (two of ν_{17} and three of ν_{27}) contain transitions affected by resonances at J'' + 1 = 81; these series are depicted in Figure 9. Upon first inspection, the magnitudes of transition displacement match between the ν_{27} $K_a = 3^+$ and ν_{17} $K_a = 9^-$ series, and it visually appears that the shape of displacement in the ν_{17} $K_a = 7^+$ plot resembles that of the ν_{27} $K_a = 4^-$, J'' + 1 = 81 displacement, perhaps affected by the steep slope on which the former is found. Such an interaction, however, is symmetry disallowed for this Coriolis-coupled system as a $\Delta K_a = 3$ (odd), $\Delta K_c = 4$ (even) interaction should only occur with a c-type Coriolis interaction.

To elucidate the appearance of local perturbations in the resonance plots, we modeled the baseline curvature of each resonance plot with a polynomial of appropriate order, excluding the highly perturbed transitions. This baseline model was subtracted from the corresponding resonance plots in Figure 9, and the resultant, baseline-flattened resonance plots are provided in Figure 10 with all x- and y-axes set at the same scale. Once the baseline is flattened, it becomes apparent that the displacements in the ν_{27} $K_a = 3^-$ and ν_{17} $K_a = 7^+$ series at J'' + 1 = 81 are involved in an a-type interaction with $\Delta K_a = 4$. The expected a-type interaction between the ν_{27} $K_a = 3^+$ and ν_{17} $K_a = 9^-$ series ($\Delta K_a = 6$) is also confirmed. Upon closer inspection, however, the displacements of transitions in these two series near J'' + 1 = 81 do not perfectly mirror one another. The red arrows in Figure 10 show the magnitude of displacement at J'' + 1 = 81 due to the a-type interaction between ν_{27} $K_a = 3^+$ and ν_{17} $K_a = 9^-$. This perturbation coincides with the b-type interaction at J'' + 1 = 81 between ν_{27} $K_a = 4^-$ and ν_{17} $K_a = 9^-$ (represented by the orange arrows). The confirmation of this interaction is provided in the "Composite," bottom-left panel in Figure 10, which shows the sum of the three resonance plots (ν_{27} $K_a = 4^-$, ν_{27} $K_a = 3^+$, and ν_{17} $K_a = 9^-$). In this plot, the displacements of all transitions involved in interactions near J'' + 1 = 81 have cancelled out, and the only remaining feature is the unrelated set of resonant transitions at J'' + 1 = 87−89.

If the experimental least-squares fit or the computational deperturbation treatment is not adequately addressing the coupling between states, the values of the vibration−rotation interaction constants (α_i) typically show characteristic large, equal, and opposite deviations for ν_{17} and ν_{27}, relative to their corresponding ground-state values. Whether or not the experimental $A_0 - A_v$ values are displaying such behavior is ambiguous in the present dyad (Table 3). The $A_0 - A_v$ values

Table 3. Vibration−Rotation Interaction and Coriolis-Coupling Constants of (Cyanomethylene)cyclopropane (5)

	Experimental	B3LYP	MP2
$A_0 - A_{17}$ (MHz)	−81.8 (12)	203	186
$B_0 - B_{17}$ (MHz)	−5.470 (18)	−2.06	−2.34
$C_0 - C_{17}$ (MHz)	−2.497127 (83)	−1.69	−1.77
$A_0 - A_{27}$ (MHz)	73.5 (12)	−230	−212
$B_0 - B_{27}$ (MHz)	−2.734 (0.018)	−3.51	−3.51
$C_0 - C_{27}$ (MHz)	−3.049301 (73)	−2.24	−2.33
$\frac{(A_0 - A_{17}) + (A_0 - A_{27})}{2}$ (MHz)	−4.1 (17)	−13.28	−13.17
$\frac{(B_0 - B_{17}) + (B_0 - B_{27})}{2}$ (MHz)	−4.102 (25)	−2.79	−2.93
$\frac{(C_0 - C_{17}) + (C_0 - C_{27})}{2}$ (MHz)	−2.77321 (11)	−1.97	−2.05
$\zeta^a_{17,27}$ (MHz)	0.633	0.584	0.578
$\zeta^b_{17,27}$ (MHz)	0.054	0.035	0.035

are large and of opposite sign, making it unclear whether this is a physically meaningful set of vibration−rotation interaction constants or if there is some residual, unaddressed a-axis coupling. It is much more apparent that the theoretical values for $A_0 - A_v$ have equal and opposite discrepancies of approximately 300 MHz, relative to their experimental counterparts using either level of theory. This indicates that whatever deperturbation treatment may have been included in the computational prediction is not sufficient for these two states. As can be seen for the $B_0 - B_v$ and $C_0 - C_v$ values as well as the average of the ν_{17} and ν_{27} vibration−rotation interaction constants, these two states are also more poorly modeled than is typically expected for both theoretical treatments.

The Coriolis coupling along the a- and b-axes cannot be modeled by simply using the first-order G_a and G_b constants. The Coriolis-coupling spectroscopic constants G_a and G_b are related to the Coriolis-coupling constant ζ values by eq 1.

$$G_x = \frac{\omega_{17} + \omega_{27}}{\sqrt{\omega_{17} \times \omega_{27}}} \zeta^x_{17,27} B^x_e \approx 2\zeta^x_{17,27} B^x_e \quad (1)$$

This relation between G and ζ is approximate in its dependence upon the harmonic frequencies of each state, in the estimate of the equilibrium rotational constants, and in the neglect of higher-order coupling terms. The experimentally estimated ζ values and their computed counterparts are presented in Table 3. Both of the theoretical values of $\zeta^a_{17,27}$ and $\zeta^b_{17,27}$ are somewhat smaller than the corresponding experimental estimates. It cannot be determined from this work whether the discrepancies in the computed and experimental values are due to incomplete theoretical treatment or an incomplete resolution of the G_a and G_b contributions to the resonances and global perturbations.

When the state mixing is sufficient to create these resonances, formally *forbidden* simultaneous transitions involving changes in both rotational and vibrational quantum numbers become allowed. Due to the relatively weak resonances of ν_{17} (A', 125 cm^{-1}) and ν_{27} (A'', 155 cm^{-1}),

https://doi.org/10.1021/acs.jpca.1c03246
J. Phys. Chem. A 2021, 125, 5601−5614

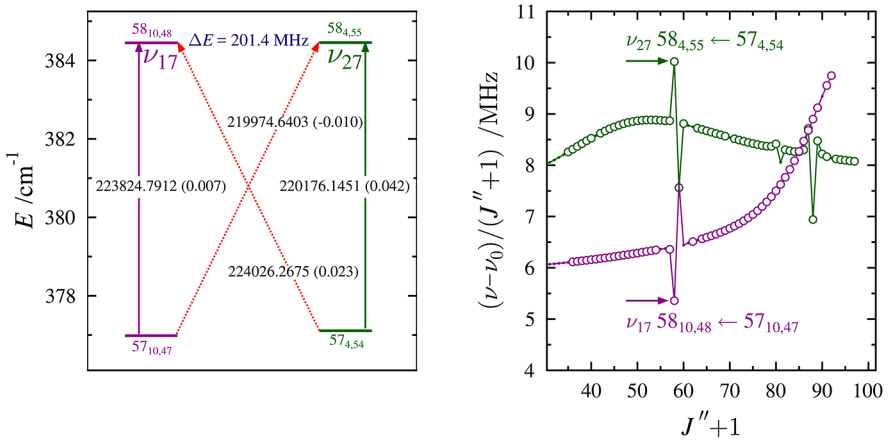

Figure 11. Energy diagram (left) depicting a representative matched pair of nominal rotation−vibration transitions between the ν_{27} (purple) and ν_{17} (green) vibrational states of (cyanomethylene)cyclopropane (**5**). Standard $^aR_{0,1}$ transitions within vibrational states are denoted by vertical arrows. The diagonal, dashed arrows indicate nominal interstate transitions that are formally forbidden but become allowed as a result of rotational energy level mixing. Values printed on each of the arrows are the corresponding transition frequency (in MHz) with its *obs.* − *calc.* value in parentheses. The marked energy separation is the energy separation between the two strongly interacting rotational energy levels. Resonance plots (right) of the K_a series of ν_{17} and ν_{27} contain the corresponding resonant transitions labeled with their quantum numbers and marked by colored arrows.

only a small number of these *forbidden* nominal interstate transitions were visible. Interstate transitions were included in the data set when they could be confidently assigned due to their intensity or in comparison to their corresponding intravibrational state transitions. In total, only nine nominal interstate transitions were included in the data set. One set of nominal interstate transitions and their intrastate counterparts are shown in Figure 11. The measured frequency of each transition and its *obs.* − *calc.* value are provided for all four transitions. All four transitions were close to their predicted intensities, and the sum of the intrastate and interstate transition frequencies differ by only 28 kHz. The low error in each individual transition and their energetic consistency provides confidence that all four transitions are properly assigned and accurately measured. The two corresponding resonant transitions are the $(J'' + 1 = 58)$ transitions from the $K_a = 4^-$ series of ν_{27} and $K_a = 10^+$ series of ν_{17} shown in Figure 8, and their resonance plots are redisplayed in Figure 11 to highlight the relation between the resonant transitions and the nominal interstate transitions. The mixing occurs with $\Delta K_a = 6$ due to the large vibrational energy difference of 30 cm^{-1} and the requirement for the rotational energy levels of the lower-energy vibrational state (ν_{17}) to catch up with the rotational energy levels of the higher-energy vibrational state (ν_{27}). For example, the $58_{10,48}$ energy level of ν_{17} and the $58_{4,55}$ energy level of ν_{27} are sufficiently close to one another (0.006720 cm^{-1} or 201.4 MHz) that strong state-mixing becomes possible. The result of the least-squares fitting of transitions involving strongly interacting energy levels results in the very accurate value determination of the energy separation between these two vibrationally excited states.

CONCLUSIONS

The first isolation of (cyanomethylene)cyclopropane (**5**) as a pure compound allowed an investigation of its gas-phase, pure rotational spectrum. The rotational constants of the ground vibrational state are very well determined and should accurately predict the rotational transitions at frequencies lower than in this work. Transitions at slightly higher frequencies than 360 GHz should also be reasonably well predicted, though with reduced accuracy as the frequency increases. These transitions provide the foundational work needed for further investigation of this molecule *via* rotational spectroscopy or radioastronomy.

The analysis of the experimentally determined spectroscopic constants in this work and many others is incomplete due to the lack of theoretical values available for comparison. The ground-state spectroscopic constants require an octic treatment of the centrifugal distortion, but there is insufficient data in the transitions measured to determine a complete set of these constants. A broader frequency range that includes transitions of higher J and K values would be necessary to reliably determine all of the octic terms. Given the present inability of theoretical methods to predict octic centrifugal distortion constants, their values in this work cannot be evaluated for their physical meaningfulness. The tactic of setting some of the octic constants to a value of 0 inherently distorts the remaining octic constants and, to a lesser extent, the sextic centrifugal distortion constants.

The impact of a lack of theoretical spectroscopic constants is more profound for the vibrationally excited states. With no method currently available to address the vibration−rotation interaction for the centrifugal distortion constants, values for these constants that cannot be sufficiently determined must be held constant at their corresponding ground-state values. In this work, computational quartic constants for ν_{17} and ν_{27} would have assisted in the initial stages of least-squares fitting by using values closer to their true values than the ground-state constants. Given the complexity of modeling the centrifugal distortion and Coriolis coupling in the same least-squares fit, computational centrifugal distortion values would allow the coupling to be addressed more efficiently early in the fitting process. To further complicate matters, the majority of the Coriolis-coupling terms cannot be predicted in a straightforward manner. In the final analysis of the spectroscopic constants, computational values of either the centrifugal distortion or Coriolis-coupling beyond those currently available would greatly expedite the fitting process and

https://doi.org/10.1021/acs.jpca.1c03246
J. Phys. Chem. A 2021, 125, 5601−5614

improve the confidence in the experimental values obtained by least-squares fitting transitions of coupled dyads and polyads.

Independent of the ambiguities with the higher-order centrifugal distortion constants and Coriolis-coupling terms, this work provides a highly accurate and precise energy difference between these two vibrationally excited states, ν_{17} and ν_{27}. Pure rotational spectroscopy, however, cannot directly determine the individual energy values of these states. Due to their isolation from the ground vibrational state, high-resolution IR spectroscopy would be necessary for accurate measurement of the energy of these fundamentals. The experimental measurement of $\Delta E_{17,27}$ serves as a benchmark for future computational estimations and, combined with the spectroscopic constants determined for (cyanomethylene)-cyclopropane (**5**) in this work, makes the fitting of the high-resolution IR spectra of ν_{17} and ν_{27} a one-variable problem.

General Experimental Methods. All commercial reagents were purchased from Sigma-Aldrich or Oakwood Chemical and used as received, unless otherwise noted. ^{1}H NMR spectra (400 or 500 MHz) and ^{13}C{^{1}H}-NMR spectra (100 or 125 MHz) were obtained in $CDCl_3$ on a Bruker 400 MHz AVANCE III or Bruker 500 MHz DCH AVANCE III spectrometer; chemical shifts (δ) are reported as ppm downfield from internal standard $SiMe_4$ or referenced to residual solvent signals. Mass spectra were acquired using electrospray ionization (ESI) or the atmospheric solids analysis probe (ASAP) on a Thermo Scientific Q-Exactive Plus mass spectrometer. IR spectra were obtained on a Bruker TENSOR Fourier transform IR instrument as neat samples using an attenuated total reflectance accessory (Bruker PLATINUM ATR).

*1-Ethoxycyclopropanol (**8**).*[28] A solution of (1-ethoxycyclopropoxy)trimethylsilane (**10**, 9.98 g, 57 mmol) in methanol (25 mL) was stirred at room temperature for 24 h. The reaction was monitored *via* ^{1}H NMR and TLC, which confirmed complete deprotection of the trimethylsilane group at 24 h. The methanol solvent was subsequently removed *in vacuo* to afford a clear, colorless oil. The crude oil was purified *via* short-path distillation to yield 1-ethoxycyclopropanol (**8**, bp = 88−90 °C at 100 Torr) as a colorless oil (5.0 g, 48.5 mmol, 85%). TLC: R_f = 0.3 (hexane/EtOAc, 4:1; $KMnO_4$). ^{1}H NMR ($CDCl_3$, 500 MHz): δ (ppm) 4.37 (br s, 1H), 3.77 (q, J = 7.2 Hz, 2H), 1.21 (t, J = 7.1 Hz, 3H), 0.98−0.87 (m, 4H). ^{13}C{^{1}H}-NMR ($CDCl_3$, 125 MHz): δ (ppm) 85.5, 62.0, 15.4, 14.2. IR (neat): (cm^{-1}) 3386 (m), 2978 (w), 1734 (m), 1460 (w), 1298 (m), 1225 (m), 1052 (m), 943 (m), 487 (w). HRMS (ESI) m/z: $[M + H]^+$ calcd for $C_5H_{11}O_2$, 103.0754; found, 103.0753.

*(Cyanomethylene)triphenylphosphorane (**9**).*[27] To a stirred solution of (cyanomethyl)triphenylphosphonium chloride (**11**, 120.4 g, 60.5 mmol) in 200 mL of deionized water was added, dropwise, an aqueous solution of sodium hydroxide (50% w/w, 10.0 mL) over 5 min at room temperature. The addition resulted in the formation of a white precipitate, and the mixture was stirred for an additional 30 min. The resulting white solid was isolated by filtration *via* a coarse glass fritted filter and dried *in vacuo* for 24 h to yield (cyanomethylene)-triphenylphosphorane (**9**, 17.0 g, 56.5 mmol, 93%). ^{1}H NMR ($CDCl_3$, 500 MHz): δ (ppm) 7.43−7.71 (m, 15H), 1.60 (s, 1H). ^{13}C{^{1}H}-NMR (125 MHz, $CDCl_3$): δ (ppm) 132.80 (d, J = 10.1 Hz), 132.57 (d, J = 3.0 Hz), 132.11 (d, J = 9.8 Hz), 129.08 (d, J = 12.4 Hz), 128.50 (d, J = 12.1 Hz), 127.43 (d, J = 91.8 Hz). Chemical shifts are consistent with previous reports.[38]

*(Cyanomethylene)cyclopropane (**5**).* To a flame-dried 250 mL single-neck round-bottom flask (cooled under a stream of N_2) was added 1-ethoxycyclopropanol (**8**, 2.07 g, 20.3 mmol), (cyanomethylene)triphenylphosphorane (**9**, 6.01 g, 20 mmol), benzoic acid (243 mg, 2 mmol, 10 mol %), and 115 mL of benzene. The reaction vessel was fitted with a water-cooled reflux condenser (with N_2 vent) and heated to reflux for 24 h. After cooling to room temperature, the flask was fitted with a fractionating column (23 cm, glass bead-packed) and a short-path distillation apparatus. Most of the benzene was removed by distillation at atmospheric pressure. To the remaining liquid (~40 mL) in the boiling flask, 100 mL of pentane was added, and the solution was cooled on ice to precipitate triphenylphosphine oxide. The resulting mixture was filtered through a fine glass frit into a separate boiling flask, and pentane was removed by short-path distillation with a fractionating column at atmospheric pressure, leaving the crude product as a bright yellow liquid. The crude product was purified *via* short-path vacuum distillation to yield (cyanomethylene)cyclopropane (**5**) (bp = 88 °C at 100 Torr) as a colorless oil (820 mg, 52%). TLC: R_f = 0.5 (pentane/diethyl ether, 6:1; $KMnO_4$). ^{1}H NMR ($CDCl_3$, 400 MHz): δ (ppm) 5.76 (p, J = 2 Hz, 1H), 1.40 (d, J = 2 Hz, 4H). ^{13}C{^{1}H}-NMR ($CDCl_3$, 100 MHz): δ (ppm) 151.9, 116.8, 90.4, 5.2, 4.1 IR (neat): (cm^{-1}) 3072 (w), 3020 (w), 2987 (w), 2221 (m), 1744 (w), 1403 (w), 1230 (w), 1058 (m), 1003 (m), 939 (m), 913 (m), 760 (s), 732 (m), 682 (m). HRMS (ESI) m/z: $[M + H]^+$ calcd for C_5H_6N, 80.0495; found, 80.0494.

■ ASSOCIATED CONTENT

Supporting Information

The Supporting Information is available free of charge at https://pubs.acs.org/doi/10.1021/acs.jpca.1c03246.

Experimental IR, ^{1}H NMR, ^{13}C NMR, and mass spectra of all compounds (PDF)

Computational chemistry output files, least-squares fitting output files from ASFIT and SPFIT (ZIP)

■ AUTHOR INFORMATION

Corresponding Authors

Robert J. McMahon − *Department of Chemistry, University of Wisconsin−Madison, Madison, Wisconsin 53706-1322, United States;* orcid.org/0000-0003-1377-5107; Email: robert.mcmahon@wisc.edu

R. Claude Woods − *Department of Chemistry, University of Wisconsin−Madison, Madison, Wisconsin 53706-1322, United States*; Email: rcwoods@wisc.edu

Authors

Brian J. Esselman − *Department of Chemistry, University of Wisconsin−Madison, Madison, Wisconsin 53706-1322, United States;* orcid.org/0000-0002-9385-8078

Samuel M. Kougias − *Department of Chemistry, University of Wisconsin−Madison, Madison, Wisconsin 53706-1322, United States;* orcid.org/0000-0002-9877-0817

Maria A. Zdanovskaia − *Department of Chemistry, University of Wisconsin−Madison, Madison, Wisconsin 53706-1322, United States;* orcid.org/0000-0001-5167-8573

Complete contact information is available at:

https://pubs.acs.org/10.1021/acs.jpca.1c03246

Notes

The authors declare no competing financial interest.

■ ACKNOWLEDGMENTS

We gratefully acknowledge the National Science Foundation for support of this project (CHE-1664912 and CHE-1954270). We thank Michael McCarthy for the loan of an amplification−multiplication chain and the Harvey Spangler Award (to B.J.E.) for support of the purchase of the corresponding zero-bias detector. We thank the following organizations and individuals for support of shared departmental facilities: Bruker AVANCE 400 NMR spectrometer (NSF CHE-1048642), Bruker AVANCE 500 NMR spectrometer (gift from Paul J. and Margaret M. Bender), and Thermo Scientific Q Exactive Plus mass spectrometer (NIH 1S10 OD020022-1).

■ REFERENCES

(1) Müller, H. S. P.; Schlöder, F.; Stutzki, J.; Winnewisser, G. The Cologne Database for Molecular Spectroscopy, CDMS: a Useful Tool for Astronomers and Spectroscopists. *J. Mol. Struct.* **2005**, *742*, 215−227.

(2) Müller, H. S. P.; Thorwirth, S.; Roth, D. A.; Winnewisser, G. The Cologne Database for Molecular Spectroscopy. *Astron. Astrophys.* **2001**, *370*, L49−L52.

(3) Zdanovskaia, M. A.; Esselman, B. J.; Lau, H. S.; Bates, D. M.; Woods, R. C.; McMahon, R. J.; Kisiel, Z. The 103 − 360 GHz Rotational Spectrum of Benzonitrile, the First Interstellar Benzene Derivative Detected by Radioastronomy. *J. Mol. Spectrosc.* **2018**, *351*, 39−48.

(4) Zdanovskaia, M. A.; Esselman, B. J.; Woods, R. C.; McMahon, R. J. The 130 − 370 GHz Rotational Spectrum of Phenyl Isocyanide (C_6H_5NC). *J. Chem. Phys.* **2019**, *151*, 024301.

(5) Dorman, P. M.; Esselman, B. J.; Woods, R. C.; McMahon, R. J. An Analysis of the Rotational Ground State and Lowest-energy Vibrationally Excited Dyad of 3-Cyanopyridine: Low Symmetry Reveals Rich Complexity of Perturbations, Couplings, and Interstate Transitions. *J. Mol. Spectrosc.* **2020**, *373*, 111373.

(6) Dorman, P. M.; Esselman, B. J.; Park, J. E.; Woods, R. C.; McMahon, R. J. Millimeter-Wave Spectrum of 4-Cyanopyridine in its Ground State and Lowest-Energy Vibrationally Excited States, ν_{20} and ν_{30}. *J. Mol. Spectrosc.* **2020**, *369*, 111274.

(7) Kougias, S. M.; Knezz, S. N.; Owen, A. N.; Sanchez, R. A.; Hyland, G. E.; Lee, D. J.; Patel, A. R.; Esselman, B. J.; Woods, R. C.; McMahon, R. J. Synthesis and Characterization of Cyanobutadiene Isomers—Molecules of Astrochemical Significance. *J. Org. Chem.* **2020**, *85*, 5787−5798.

(8) Zdanovskaia, M. A.; Dorman, P. M.; Orr, V. L.; Owen, A. N.; Kougias, S. M.; Esselman, B. J.; Woods, R. C.; McMahon, R. J. Rotational Spectra of Three Cyanobutadiene Isomers (C_5H_5N) of Relevance to Astrochemistry and Other Harsh Reaction Environments. *J. Am. Chem. Soc.*, in press.

(9) Zdanovskaia, M. A.; Esselman, B. J.; Kougias, S. M.; Patel, A. R.; Woods, R. C.; McMahon, R. J. The 130 − 370 GHz Rotational Spectrum of 2-Cyano-1,3-Butadiene − A Molecule of Astrochemical Relevance. Manuscript submitted.

(10) Charnley, S. B.; Kuan, Y.-J.; Huang, H.-C.; Botta, O.; Butner, H. M.; Cox, N.; Despois, D.; Ehrenfreund, P.; Kisiel, Z.; Lee, Y.-Y.; et al. Astronomical Searches for Nitrogen Heterocycles. *Adv. Space Res.* **2005**, *36*, 137−145.

(11) McGuire, B. A.; Burkhardt, A. M.; Kalenskii, S.; Shingledecker, C. N.; Remijan, A. J.; Herbst, E.; McCarthy, M. C. Detection of the Aromatic Molecule Benzonitrile (*c*-C_6H_5CN) in the Interstellar Medium. *Science* **2018**, *359*, 202−205.

(12) McGuire, B. A.; Loomis, R. A.; Burkhardt, A. M.; Lee, K. L. K.; Shingledecker, C. N.; Charnley, S. B.; Cooke, I. R.; Cordiner, M. A.; Herbst, E.; Kalenskii, S.; et al. Detection of Two Interstellar Polycyclic Aromatic Hydrocarbons via Spectral Matched Filtering. *Science* **2021**, *371*, 1265−1269.

(13) McCarthy, M. C.; Lee, K. L. K.; Loomis, R. A.; Burkhardt, A. M.; Shingledecker, C. N.; Charnley, S. B.; Cordiner, M. A.; Herbst, E.; Kalenskii, S.; Willis, E. R.; et al. Interstellar Detection of the Highly Polar Five-Membered Ring Cyanocyclopentadiene. *Nat. Astron.* **2021**, *5*, 176−180.

(14) Sun, B. J.; Huang, C. H.; Chen, S. Y.; Chen, S. H.; Kaiser, R. I.; Chang, A. H. H. Theoretical Study on Reaction Mechanism of Ground-State Cyano Radical with 1,3-Butadiene: Prospect of Pyridine Formation. *J. Phys. Chem. A* **2014**, *118*, 7715−7724.

(15) Morales, S. B.; Bennett, C. J.; Le Picard, S. D.; Canosa, A.; Sims, I. R.; Sun, B. J.; Chen, P. H.; Chang, A. H. H.; Kislov, V. V.; Mebel, A. M.; et al. A Crossed Molecular Beam, Low-Temperature Kinetics, and Theoretical Investigation of the Reaction of the Cyano Radical (CN) with 1,3-Butadiene (C_4H_6). A Route to Complex Nitrogen-Bearing Molecules in Low-Temperature Extraterrestrial Environments. *Astrophys. J.* **2011**, *742*, 26.

(16) Mishra, P.; Fritz, S. M.; Herbers, S.; Mebel, A. M.; Zwier, T. S. Gas-phase Pyrolysis of *trans* 3-Pentenenitrile: Competition Between Direct and Isomerization-Mediated Dissociation. *PCCP Phys. Chem. Chem. Phys.* **2021**, *23*, 6462−6471.

(17) McCarthy, M. C.; Lee, K. L. K.; Carroll, P. B.; Porterfield, J. P.; Changala, P. B.; Thorpe, J. H.; Stanton, J. F. Exhaustive Product Analysis of Three Benzene Discharges by Microwave Spectroscopy. *J. Phys. Chem. A* **2020**, *124*, 5170−5181.

(18) Tsukamoto, A.; Lichtin, N. N. Reactions of Active Nitrogen with Organic Substrates. I. The Monomeric Products of the Reaction with 1,3-Butadiene. *J. Am. Chem. Soc.* **1962**, *84*, 1601−1605.

(19) Thaddeus, P.; Vrtilek, J. M.; Gottlieb, C. A. Laboratory and Astronomical Identification of Cyclopropenylidene, C_3H_2. *Astrophys. J.* **1985**, *299*, L63−L66.

(20) Hollis, J. M.; Remijan, A. J.; Jewell, P. R.; Lovas, F. J. Cyclopropenone (*c*-H_2C_3O): A New Interstellar Ring Molecule. *Astrophys. J.* **2006**, *642*, 933−939.

(21) Dickens, J. E.; Irvine, W. M.; Ohishi, M.; Ikeda, M.; Ishikawa, S.; Nummelin, A.; Hjalmarson, Å. Detection of Interstellar Ethylene Oxide (*c*-C_2H_4O). *Astrophys. J.* **1997**, *489*, 753−757.

(22) McGuire, B. A.; Carroll, P. B.; Loomis, R. A.; Finneran, I. A.; Jewell, P. R.; Remijan, A. J.; Blake, G. A. Discovery of the Interstellar Chiral Molecule Propylene Oxide (CH_3CHCH_2O). *Science* **2016**, *352*, 1449−1452.

(23) Gardner, F. F.; Winnewisser, G. The Detection of Interstellar Vinyl Cyanide (Acrylonitrile). *Astrophys. J.* **1975**, *195*, L127−L130.

(24) Lovas, F. J.; Remijan, A. J.; Hollis, J. M.; Jewell, P. R.; Snyder, L. E. Hyperfine Structure Identification of Interstellar Cyanoallene toward TMC-1. *Astrophys. J.* **2006**, *637*, L37−L40.

(25) Broten, N. W.; MacLeod, J. M.; Avery, L. W.; Friberg, P.; Hjalmarson, A.; Hoglund, B.; Irvine, W. M. The Detection of Interstellar Methylcyanoacetylene. *Astrophys. J.* **1984**, *276*, L25−L29.

(26) Wilson, C. L. 17. Reactions of Furan compounds. Part IV. High-Temperature Decomposition of the Vapours of Tetrahydrofuronitrile and Methyl Tetrahydrofuroate to Give 2,3-Dihydrofuran and Cyclopropanealdehyde. *J. Chem. Soc.* **1945**, 58−61.

(27) Mauduit, M.; Kouklovsky, C.; Langlois, Y. Cyanomethylene Cyclopropane, a Useful Dipolarophile and Dienophile in [2+3] and [2+4] Cycloadditions. *Tetrahedron Lett.* **1998**, *39*, 6857−6860.

(28) Kleinbeck, F.; Toste, F. D. Gold(I)-Catalyzed Enantioselective Ring Expansion of Allenylcyclopropanols. *J. Am. Chem. Soc.* **2009**, *131*, 9178−9179.

(29) Amberger, B. K.; Esselman, B. J.; Stanton, J. F.; Woods, R. C.; McMahon, R. J. Precise Equilibrium Structure Determination of Hydrazoic Acid (HN_3) by Millimeter-wave Spectroscopy. *J. Chem. Phys.* **2015**, *143*, 104310.

(30) Esselman, B. J.; Amberger, B. K.; Shutter, J. D.; Daane, M. A.; Stanton, J. F.; Woods, R. C.; McMahon, R. J. Rotational Spectroscopy

of Pyridazine and its Isotopologs from 235−360 GHz: Equilibrium Structure and Vibrational Satellites. *J. Chem. Phys.* **2013**, *139*, 224304.
(31) Kisiel, Z.; Pszczółkowski, L.; Drouin, B. J.; Brauer, C. S.; Yu, S.; Pearson, J. C.; Medvedev, I. R.; Fortman, S.; Neese, C. Broadband Rotational Spectroscopy of Acrylonitrile: Vibrational Energies from Perturbations. *J. Mol. Spectrosc.* **2012**, *280*, 134−144.
(32) Kisiel, Z.; Pszczółkowski, L.; Medvedev, I. R.; Winnewisser, M.; De Lucia, F. C.; Herbst, E. Rotational Spectrum of *trans*−*trans* Diethyl Ether in the Ground and Three Excited Vibrational States. *J. Mol. Spectrosc.* **2005**, *233*, 231−243.
(33) Pickett, H. M. The Fitting and Prediction of Vibration-rotation Spectra with Spin Interactions. *J. Mol. Spectrosc.* **1991**, *148*, 371−377.
(34) Kisiel, Z. PROSPE—Programs for ROtational SPEctroscopy. http://info.ifpan.edu.pl/?kisiel/prospe.htm (accessed March 04, 2021).
(35) Frisch, M. J.; Trucks, G. W.; Schlegel, H. B.; Scuseria, G. E.; Robb, M. A.; Cheeseman, J. R.; Scalmani, G.; Barone, V.; Petersson, G. A.; Nakatsuji, H.; et al. *Gaussian 16*, rev C.01, Gaussian, Inc.: Wallingford, CT, USA, 2016.
(36) Schmidt, J. R.; Polik, W. F. *WebMO Enterprise*, version 20.0; WebMO LLC: Madison, WI, USA, 2020; http://www.webmo.net (accessed April 2021).
(37) Amberger, B. K.; Esselman, B. J.; Woods, R. C.; McMahon, R. J. Millimeter-wave Spectroscopy of Carbonyl Diazide, $OC(N_3)_2$. *J. Mol. Spectrosc.* **2014**, *295*, 15−20.
(38) Aitken, R. A.; Al-Awadi, N. A.; El-Dusouqui, O. M. E.; Farrell, D. M. M.; Kumar, A. Synthesis, Thermal Reactivity, and Kinetics of Stabilized Phosphorus Ylides. Part 2: [(Arylcarbamoyl)(cyano)-methylene]Triphenylphosphoranes and Their Thiocarbamoyl Analogues. *Int. J. Chem. Kinet.* **2006**, *38*, 496−502.

https://doi.org/10.1021/acs.jpca.1c03246
J. Phys. Chem. A 2021, 125, 5601−5614